Modelling Delamination in Fibre-Reinforced Composites subjected to Through-Thickness Compression by an adapted Cohesive Law

Moritz Kuhtz[1], Johannes Gerritzen[1], Jens Wiegand[2], Andreas Hornig[1,3,4], Maik Gude[1]

[1]TUD Dresden University of Technology, Institute of Lightweight Engineering and Polymer Technology, Holbeinstraße 3, 01307 Dresden
[2]COMPACT Composite Impact Engineering, 12 Gateway Mews, London N11 2UT
[3]Center for Scalable Data Analytics and Artificial Intelligence (ScaDS.AI) Dresden/Leipzig, Germany
[4]University of Oxford, Department of Engineering Science, Parks Road, Oxford OX1 3PJ, UK

1 Introduction

A special form of failure in impact loaded Fibre-Reinforced Composites (FRP) structures is delamination, in which individual layers of a laminate get separated from one another. In contrast to the continuum mechanically formulated models of damage mechanics, the description of delamination processes is based on concepts of fracture mechanics. Here, delamination initiation is due to interlaminar stresses [1], whereby the tolerable interlaminar shear stresses can be increased by a simultaneous through thickness compression (TTC) [2-4]. Furthermore, an increase in the critical energy release rate with increasing out-of-plane compressive load is described [5-6]. Failure to consider the compressive superposition can lead to an overestimation of the delamination failure in impact loaded FRP structures such as three-point bending beams [7].
In the study presented here, an LS-DYNA user material is introduced that accounts for both the increase in interlaminar shear strength and the critical energy release rate. The material model is verified using a single element test. Finally, the failure behaviour of a three-point bending beam with the LS-DYNA user material is investigated and compared with an existing LS-DYNA material model.

2 Modelling Delamination in LS-DYNA

Simulating the delamination behaviour of adjacent single plies of an FRP composite, cohesive zone approaches are widely used, which allow both an evaluation of the delamination initiation and a description of its growth. The modelling is achieved either via contact or element formulations with distinct material models (Fig. 1). In general, the result quality of the cohesive elements is higher than that of the contact formulations [8], which is why the material models for these elements are examined here.

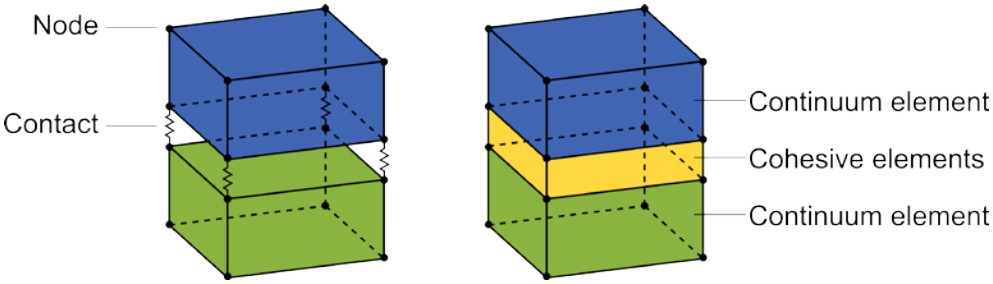

Fig.1: Approaches for cohesive zone modelling: contact (left) or material models.

2.1 Cohesive Element Material Model

Table 1 shows the material models for cohesive elements implemented in LS-DYNA R13. For modelling the delamination behaviour of carbon fibre reinforced epoxy resins, which show a very brittle failure behaviour, cohesive approaches with bilinear stress-separation progression are particularly suitable. Since multilayer composites do not show crack closure, cohesive approaches with irreversible change of state are preferable for describing the delamination behaviour. With regard to the application to the

design of impact-loaded composite beams with superimposed delamination stresses, a consideration of the mixed mode stress is necessary. Therefore, MAT 138 is chosen as the starting point for this work. It is extended by the consideration of TTC superposition and implemented as a LS-DYNA user material.

*MAT	Traction Separation Law	Crack closure	Mixed Mode	Strain rate dependency	Through thickness compression
138	bilinear	impossible	Power Law	-	-
184	linear	impossible	-	-	-
185	trilinear	possible	-	-	-
186	user defined	impossible	Power Law	-	-
240	trilinear	impossible	Power Law	logarithmic (stress) and exponential (SERR)	-

Table 1: Cohesive Material Models in LS-DYNA R13

2.2 Influence of TTC

The material model ***MAT_COHESIVE_MIXED_MODE** (*MAT138) can be used to predict the delamination behaviour under a superposition of out-of-plane tensile σ_3 and shear stresses $\tau_{II} = \sqrt{(\tau_{13})^2 + (\tau_{23})^2}$. Kellner [9] provides a code for an LS-DYNA user material model which, like *MAT138, is based on the work of Dávila and Camanho [10]. The influence of a compressive stress in the thickness direction σ_3 is not taken into account in both material models. However, recent works show an increase of the interlaminar properties like shear strength R_{II} and the mode II critical energy release rate $\mathcal{G}_{IIc}$ with increasing compressive stress σ_3 [11]. While Catalanotti et al. use the single parameter η to model the impact of a compressive stress on both strength and critical interlaminar energy release rate, here, two independent parameters η_R and $\eta_{\mathcal{G}}$ are chosen in order to take into account the different phenomena causing delamination initiation and growth:

$$R_{II} = R_{II0}\sqrt{(1 - \eta_R\ \sigma_3)} = \alpha_R\, R_{II0}\,, \text{ for } \sigma_3 < 0, \tag{1}$$

$$\mathcal{G}_{IIc} = \mathcal{G}_{IIc0}\left(1 - \eta_{\mathcal{G}}\ \sigma_3\right) = \alpha_{\mathcal{G}}\, \mathcal{G}_{IIc0}\,, \text{ for } \sigma_3 < 0, \tag{2}$$

where R_{II0} and $\mathcal{G}_{IIc0}$ are the interlaminar strength and critical energy release rates without superimposed compressive stress. This approach is used to develop a new cohesive zone model that factors the increase in interlaminar properties with increasing interlaminar compressive stress.

3 LS-DYNA user material model

3.1 Implementation

The proposed material model extensions are implemented as Fortran subroutine for usage as LS-DYNA ***MAT_USER_DEFINED_MATERIAL_MODELS** with an explicit time integration scheme. The accompanying source code is available online [12]. The principal functionality of the subroutine is illustrated in Fig.2:. First, the adaption parameters α_R and $\alpha_{\mathcal{G}}$ are calculated in case of TTC, otherwise they are set to 1, indicating no changes to the original behaviour. Next, they are applied to strength and critical energy release rate respectively and the dependent variables δ_{II0} and u_{td} are updated accordingly. In the following steps, the loading scenario is assessed and in case of through thickness tension the influence of mode-mixity β is taken into account. For numerical stability, a mathematically equivalent but rearranged formulation has been chosen for the implementation of δ_F^{μ}. The modifications prevent numerical instabilities in edge cases such as $0 < \delta_3 \ll 1$, leading to very large values for β. With the adapted material parameters and determined loading conditions, the element is checked for final failure and crack initiation. In the former case the element is immediately deleted, in the latter a linear damage evolution is applied, leading to an isotropic reduction of the material's stiffness. Finally, the stress responses are calculated based on the given separations and the resulting material state.

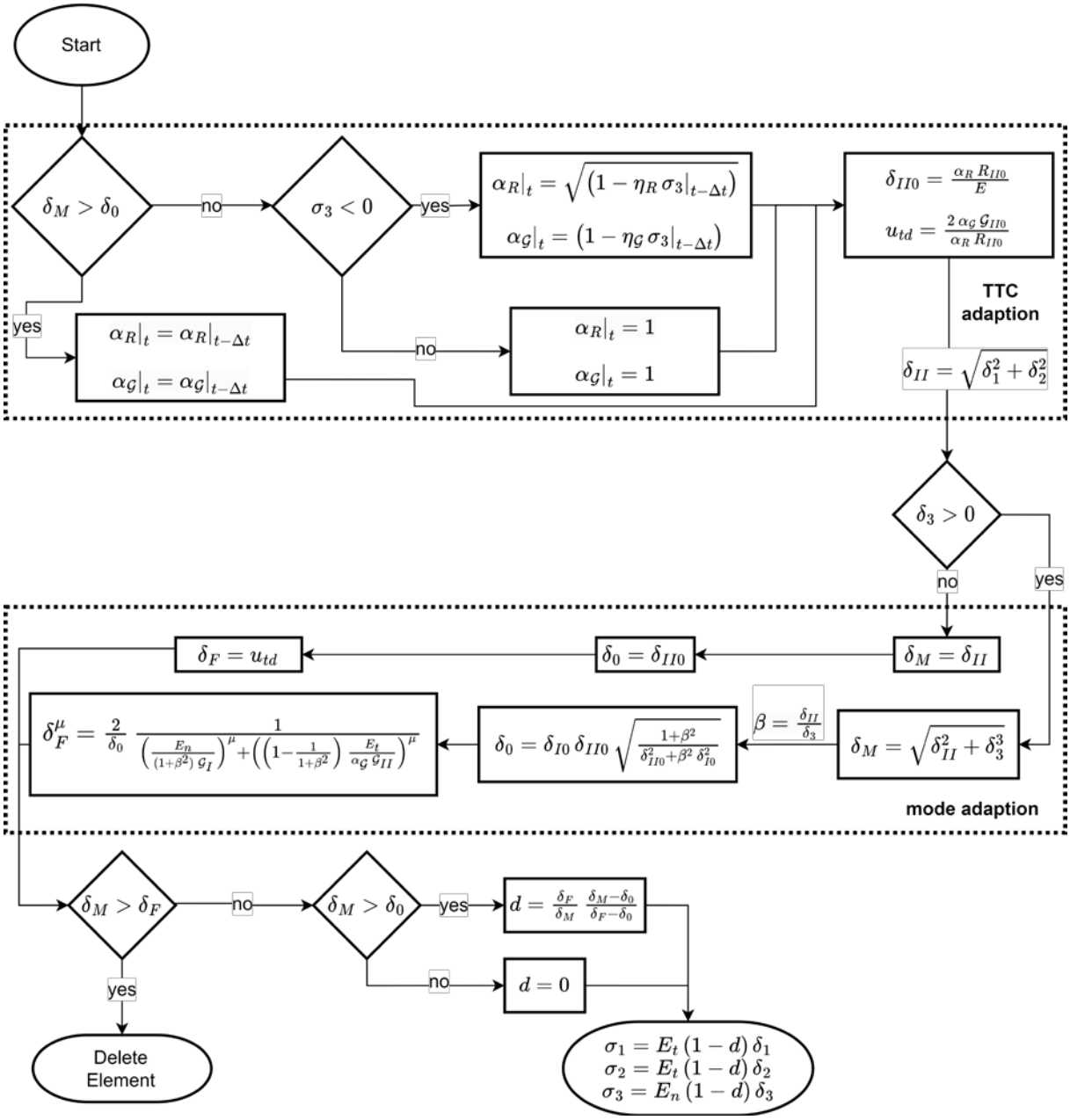

Fig.2: Flow Chart of subroutine procedure

3.2 Verification by a single element test

To verify the implemented material model, a single-element test is performed to assess the Mode II failure behaviour under different compressive loads. With fixed node displacements of the lower nodes, a compressive force F_3 is first applied to the upper nodes. Subsequently, a separation between the upper and lower node rows is initiated by a displacement boundary condition δ_1.

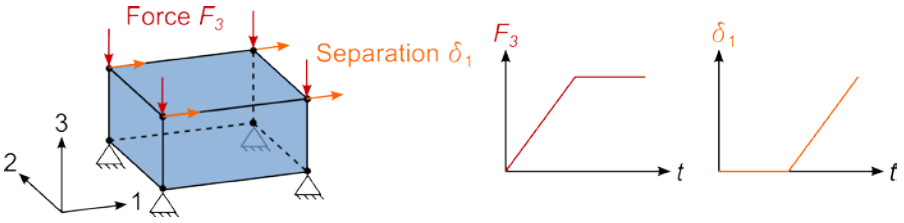

Fig.3: Single Element Test to verify the mode II failure behaviour under through thickness compression.

Table 2 shows the material parameters used.

Mode	Parameter	Symbol	Quantity	Unit
Mode I	Stiffness	K_I	$5.0 \cdot 10^6$	$\mathrm{N/mm^3}$
	Strength	R_I	35.5	MPa
	Energy release rate	$\mathcal{G}_{Ic}$	0.86	$\mathrm{N/mm}$
Mode II	Stiffness	K_{II}	$2.5 \cdot 10^6$	$\mathrm{N/mm^3}$
	Strength	R_{II}	42.6	MPa
	Energy release rate	$\mathcal{G}_{IIc}$	1.74	$\mathrm{N/mm}$
	Scale factor strength	η_R	0.0035	$\mathrm{MPa^{-1}}$
	Scale factor energy release rate	$\eta_\mathcal{G}$	0.0035	$\mathrm{MPa^{-1}}$

Table 2: Cohesive Material Model parameters of the material model

Fig. 4 left shows traction separation curves for different parameter combinations of η_R and $\eta_\mathcal{G}$ at a superimposed compressive stress $\sigma_3 = -50\,\mathrm{MPa}$. Compared to *MAT138 ($\eta_R = \eta_\mathcal{G} = 0$), an increase in shear strength due to compressive superposition ($\eta_R > 0, \eta_\mathcal{G} = 0$) results in a lower maximum separation, implying a brittle failure behaviour. In contrast, a much tougher delamination behaviour ($\eta_R = 0, \eta_\mathcal{G} > 0$) results, as indicated by a larger maximum displacement, when only the critical energy release rate due to pressure superposition is increased. It can be seen that the parameter η_R effects the stress maximum, whereas the damage behaviour is determined by the parameter $\eta_\mathcal{G}$. If the same values are used for both scaling parameters ($\eta_R = \eta_\mathcal{G} > 0$), this leads to a parallel shift of the softening curve.

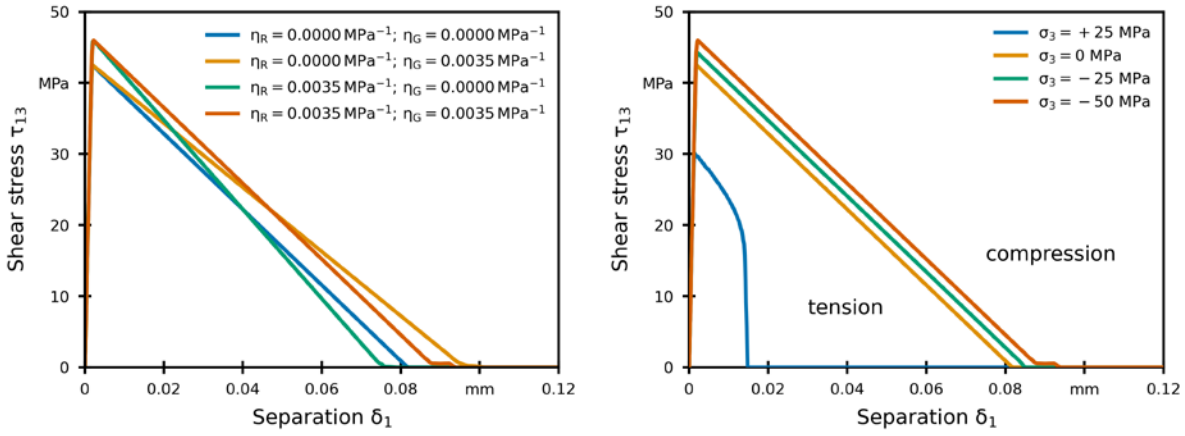

Fig.4: Traction Separation Curve in Mode II of a single cohesive element test: left: different scale factors and out-of-plane compressive load of stress $\sigma_3 = 50\,MPa$ right: different out-of-plane loads and constant scale factors $\eta_R = \eta_\mathcal{G} = 0.0035\,MPa^{-1}$

Fig. 4 right shows the stress separation curves of the developed material model at different out-of-plane stresses for the scale factors $\eta_R = \eta_\mathcal{G} = 0.0035\,\mathrm{MPa^{-1}}$. When compressive stress occurs in the thickness direction, the damage initiation is shifted to higher shear stresses and separations according to the implemented equations 1 and 2. For superimposed tensile stresses, on the other hand, the failure behaviour occurs according to the quadratic mixed mode failure [13]. Due to the lower energy release rate in mode I $\mathcal{G}_{Ic}$, the damage curve in mixed mode is progressive and non-linear.

4 Three Point Bending Test

4.1 Model set-up

The deformation and failure behaviour of the FRP beam is modelled using a three-dimensional FE model (Fig. 5). Delamination is modelled using cohesive elements using the user-defined LS-DYNA material model presented here. The composite is represented by fully integrated solid hexahedral elements (type -1). The element size in the x-direction was chosen to be 0.25 mm, with each single composite ply discretised by three elements (z -direction). The thickness of the cohesive elements is 0.05 mm. The experimental investigations [14] show no change in the deformation and failure behaviour in the test specimen width direction (y-direction), which is why only an eighth of the test specimen is modelled here with three elements.
The impactor is modelled as an elastic body of steel with an initial velocity of 3132 $^{\mathrm{mm}}/_{\mathrm{s}}$ in negative z-direction. Its characteristic element size in contact area is 0.25 mm, equal to the element size of the test specimen, and its density is adjusted so that the total mass is 250 g (one eighth of 2 kg). The supports are modelled as rigid bodies and are fixed in space with all degrees of freedom so that the time step is not influenced by their element size. For a good representation of the geometrically curved contact area, the supports are modelled with a smaller characteristic element size of 0.1 mm. Table 3 gives an overview of the number and type of elements in the structural model.

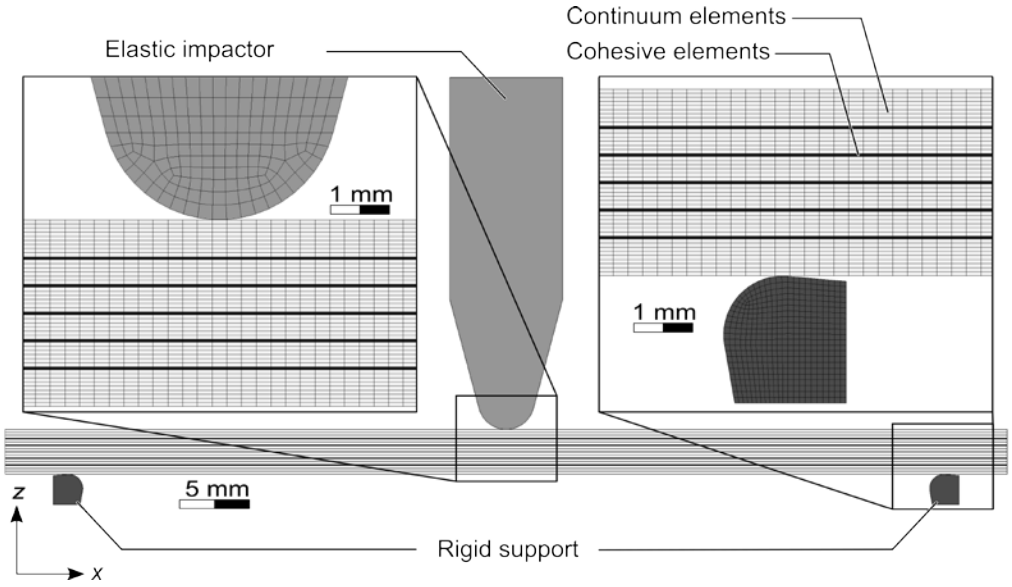

Fig.5: LS-DYNA model of a three point bending test.

A two-sided surface-to-surface contact is used as contact formulation, which maps the curved contact surfaces by smooth functions [15]. In addition, an eroding contact is implemented that acts on the exposed surfaces in the event of element deletion and thus prevents fragments of the test specimen from penetrating.

Body	Element type	Element formulation	Material model	# elements
Support	Solid	1	20	6650
Impactor	Solid	1	1	6573
Specimen	Solid	-1	58	35658
	Solid	19	user mat	4245
			sum:	53126

Table 3: Cohesive Material Model parameters of the user mat

4.2 Structural response

Figure 6 shows the Force-Displacement curve of the three point bending model with four different modelling approaches: Figure 6a) illustrates the force-displacement curve of the model without cohesive elements while Figure 6b) shows force-displacement curve for the model with *MAT138 cohesive elements. Figures 6c) and d) illustrate the force-displacement curves for the two user material models [9] and [12], respectively.

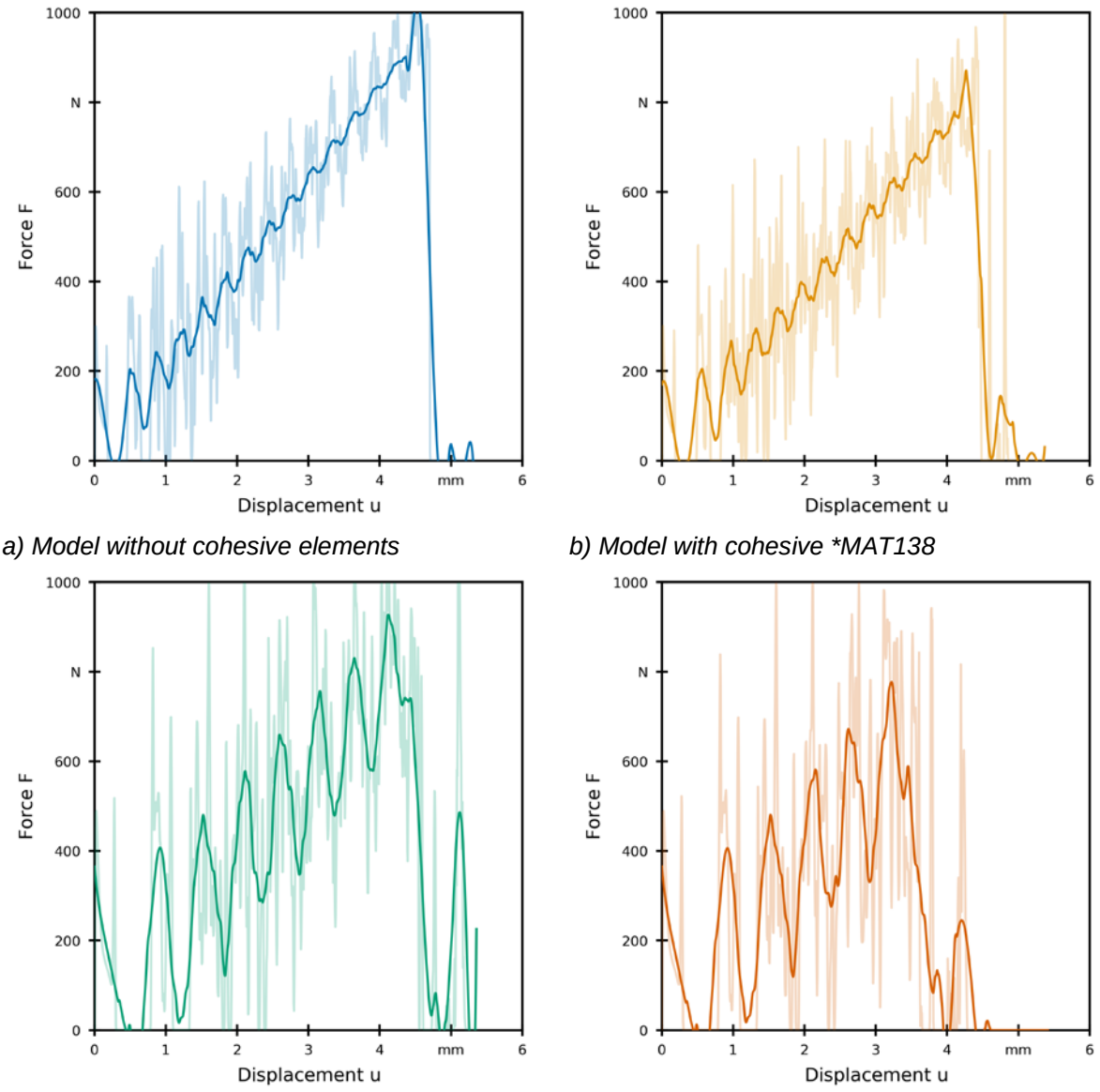

a) Model without cohesive elements

*b) Model with cohesive *MAT138*

c) Model with user material cohesive from [9]

d) Model with user material cohesive from [12]

Fig.6: Force-Displacement curve of the three point bending model

The rapid impact on the test specimen generates compressive stress waves in both bodies, which lead to high initial force peaks. Moreover the impact slows down the impactor somewhat and accelerate the test specimen. Due to its lower mass, the test specimen is accelerated in such a way that the deformation speed is higher than the speed of the impactor and both bodies briefly lift off from each other again. This phenomenon becomes clear when the contact force drops to zero and is confirmed by the experimental investigations [14].

A comparison of these results to the force-displacement curve without cohesive elements suggests that part of the noisy force signal is due to the modelling with cohesive elements. The cohesive elements represent a change in the propagation medium of the compressive stress waves due to their altered stiffness properties. Compressive stress waves are partially reflected at such impedance changes and run back as tensile stress waves [16]. On the one hand, the returning tensile stress waves reflected at

the different rows of cohesive elements overlap each other. On the other hand, these tensile stress waves overlap with the compressive stress waves that are reintroduced, which together lead to a large noise of the contact force. This suggests that the stresses resulting from this wave propagation are calculated differently in the user material model than in the cohesive elements with *MAT138. The large force amplitudes lead to the tensile or compressive strength of the continuum elements being exceeded at an early stage and thus to an earlier failure of the structure compared to the models without cohesive elements or with *MAT138 elements.

Figure 7 shows the stress distribution σ_3 and $\boldsymbol{\tau_{13}}$under the impactor as well as the resulting peak stress reached flag and damage variable d d at t $= 1.8 \cdot 10^{-5}$ s, which represents nearly the first force peak at a displacement $u = 0.0055$ mm.

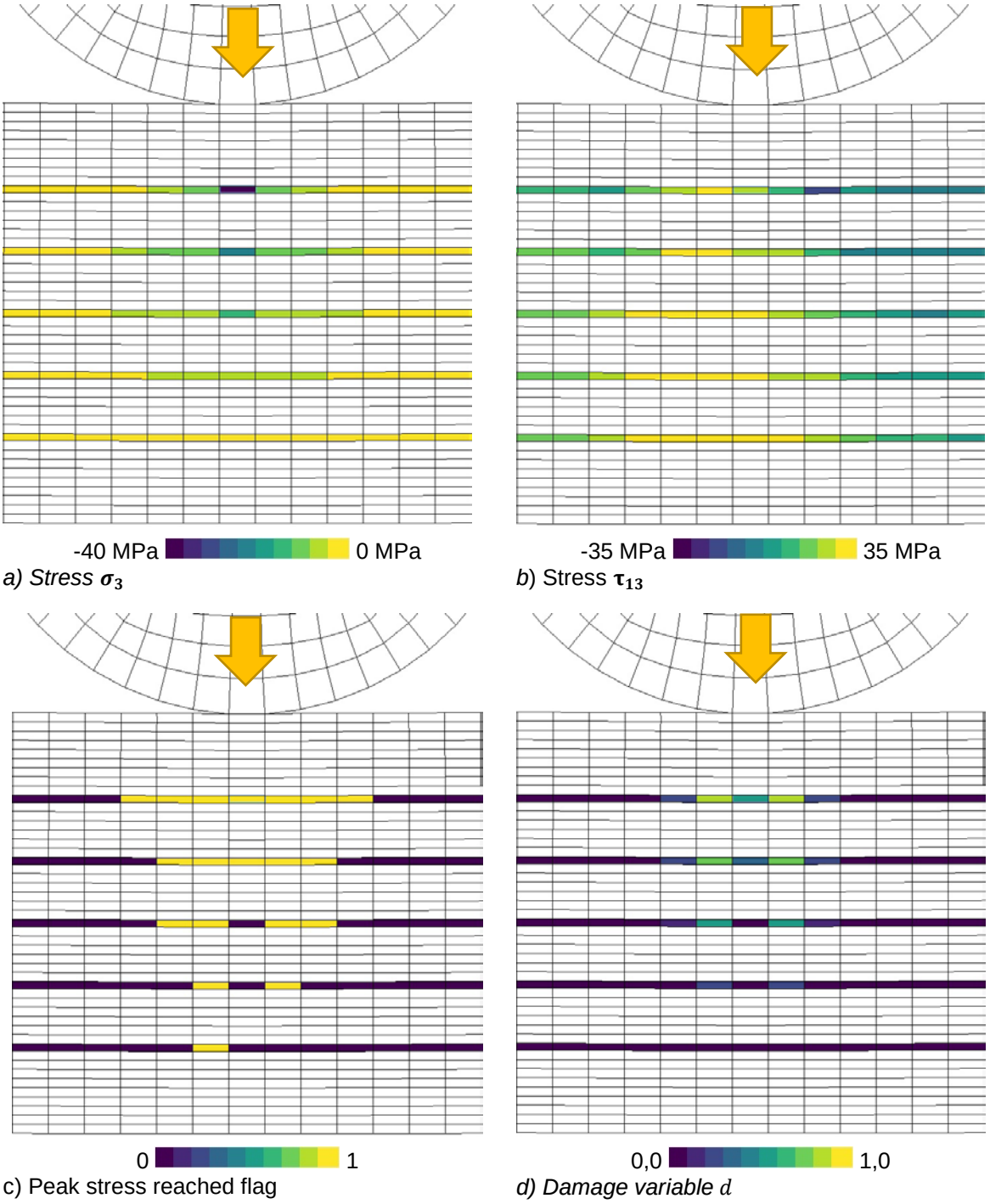

a) Stress $\boldsymbol{\sigma_3}$ *b*) Stress $\boldsymbol{\tau_{13}}$

c) Peak stress reached flag *d) Damage variable* d

Fig.7: Stress distribution σ_3 *and* τ_{13} *under the impactor and resulting peak stress flag and damage variable* d *at* $t = 1.8 \cdot 10^{-5}$ *s*

The cohesive elements have a compressive stress in the 3-direction σ_3 due to the load effect of the impactor, which is also calculated in the neighbouring continuum elements (is not shown in Figure 7). However, a large shear stress is calculated in the cohesives, which is slightly below the strength. The user material model outputs a history variable that indicates whether the maximum stresses have been reached. The variable for the peak stress reached flag is already 1 for many elements below the impactor and damage d is calculated. This damage initiation leads to a lowering of the mechanical properties. In case of failure of the neighbouring continuum elements, these low remaining mechanical properties lead to an implausible delamination failure.

5 Summary

Delamination is a significant and highly complex failure mode of FRP. Its accurate prediction still poses a major challenge, leading to larger safety factors than necessary thus limiting exploitation of the full lightweight potential of FRP in many applications. In this work, an addition to state of the art models for delamination prediction has been presented. It captures the toughening influence of TTC on the debonding behaviour of FRP. By allowing for separate scaling of initial strength and critical energy release rate, it becomes possible to model the interaction between the phenomena leading to delamination initiation and growth. The theoretical capabilities of the developed material model have been verified using single element tests, in which the influence of both novel model parameters as well as the influence of TTC has been demonstrated. Furthermore, the model has been used in structural analyses of low velocity three point bending tests. Here, the influence of the modifications has not come into effect significantly. This can potentially be attributed to the large dynamic force spikes throughout the simulation which lead to premature overstressing of the interface and thus delamination. Future work will focus on robustifying the presented model against unphysical short-term loading spoiling the entire model behaviour.

6 Acknowledgements

The authors gratefully acknowledge the financial support for this research provided by the European Union (NextGenerationEU) and the Federal Ministry for Economic Affairs and Climate Action under grant agreement no. 19S22006N (“Digitalization for Sustainability” - DigiTain). The results are also partially based upon work from COST Action HISTRATE (Composites under HIgh STRAin raTEs loading: a route to certification-by-analysis), CA21155, supported by COST (European Cooperation in Science and Technology).

7 Literature

[1] Hashin, Z.: Failure criteria for unidirectional fiber composites. Journal of Applied Mechanics, Transactions ASME 47 (1980), Nr. 2, S. 329–334. https://doi.org/10.1115/1.3153664.

[2] Hou, J.; Petrinic, N.; Ruiz, C.: A delamination criterion for laminated composites under low-velocity impact. Composites Science and Technology 61 (2001), Nr. 14, S. 2069–2074. https://doi.org/10.1016/S0266-3538(01)00128-2

[3] Xiao, J. R.; Gama, B. A.; Gillespie, J. W.: Progressive damage and delamination in plain weave S-2 glass/SC-15 composites under quasi-static punch-shear loading. Composite Structures 78 (2007), 2, pp. 182–196. https://doi.org/10.1016/j.compstruct.2005.09.001

[4] Düreth, C.; Weck, D.; Böhm, R.; Thieme, M.; Gude, M.; Wolf, C.; Henkel, S.; Biermann, H.: Interlaminar shear strength enhancement under out-of-plane compression of fabric reinforcements - a review on meso and macro scale. In Proceedings of the 18th European Conference on Composite Materials, Athens, Greece,25–28 June 2018. https://www.researchgate.net/publication/326368996, available on 30th May 2023

[5] Bing, Q.; Sun, C.T.: Effect of compressive transverse normal stress on mode II fracture toughness in polymeric composites. International Journal of Fracture. 145, 89–97 (2007) https://doi.org/10.1007/s10704-007-9103-4

[6] Li, X.; Hallett, S.R., Wismon, M.R.: Predicting the effect of through-thickness compressive stress on delamination using interface elements. Composites Part A: Applied Science and Manufacturing. 39, 218-230 (2008). https://doi.org/10.1016/j.compositesa.2007.11.005

[7] Kuhtz, M.; Richter, J.; Wiegand, J.; Langkamp, A.; Hornig, A.; Gude, M.: Concepts for Increased Energy Dissipation in CFRP Composites Subjected to Impact Loading Conditions by Optimising Interlaminar Properties. Aerospace 2023, 10, 248. https://doi.org/10.3390/aerospace10030248

[8] Dogan, F.; Hadavinia, H.; Donchev, T.; Bhonge, P.: Delamination of impacted composite structures by cohesive zone interface elements and tiebreak contact. Open Engineering 2 (2012), 4, 612–626. https://doi.org/10.2478/s13531-012-0018-0
[9] Kellner, L: " How To - user defined material models with LS-Dyna on Windows", https://www.researchgate.net/publication/327623424_How_To_-_user_defined_material_models_with_LS-Dyna_on_Windows, available on 30th May 2023
[10] C. Dávila and P. Camanho, “Decohesion Elements using Two and Three-Parameter Mixed Mode Criteria,” in American Helicopter Society Conference, Williamsburg, VA, 2001. https://ntrs.nasa.gov/api/citations/20020010916/downloads/20020010916.pdf, available on 30th May 2023
[11] Catalanotti, G.; Furtado, C.; Scalici, T.; Pitarresi, G.; van der Meer, F.P.; Camanho, P.P.: The effect of through-thickness compressive stress on mode II interlaminar fracture toughness, Composite StructuresVolume 182 (2017), 153-163. DOI: 10.1016/j.compstruct.2017.09.014
[12] https://gitlab.hrz.tu-chemnitz.de/s7768198--tu-dresden.de/ls-dyna-umat-ttc-cohesive
[13] Hahn, H. T.: A Mixed-Mode Fracture Criterion for Composite Materials. Journal of Composites, Technology and Research 5 (1983), Nr. 1, S. 26–29
[14] Kuhtz, M.; Hornig, A.; Richter, J.; Gude, M.: Increasing the structural energy dissipation of laminated fibre composite materials by delamination control. Materials & Design 156, 93-102 (2018). https://doi.org/10.1016/j.matdes.2018.06.039
[15] Stelzmann, U.: Robuste und effiziente Kontaktmodellierungen in LS-DYNA: Wie gut sind die neuen Optionen? ANSYS Conference & 30. CADFEM Users‘ Meeting 2012. http://www1.beuth-hochschule.de/~kleinsch/Expl_FEM/2012_Explizit_Kontakte_UM.pdf, available on 30th May 2023
[16] Nitschke, S.; Hornig, A.; Gude, M.: Electro-mechanical test rigs for analysing impact induced wave propagation in composite materials. In Proceedings of the 18th European Conference on Composite Materials, Athens, Greece,25–28 June 2018.